



RESEARCH ARTICLE

Biosynthesis of ZnO nanoparticles using the young fruit of *Borassus flabellifer*: Characterization and photocatalytic removal of biohazardous safranin-O dye using solar irradiation

Goutam Mandal^{1*}, Baibaswata Bhattacharjee²

Abstract

Here, ZnO nanostructures were synthesized for the first time from the young fruit of the *Borassus flabellifer*. X-ray diffraction study revealed that the unit cell of ZnO was hexagonal with particle size 39.83 nm. The field-emission scanning electron microscope (FESEM) images showed that spherical nanoparticles were formed. A sharp absorption peak was seen at 375 nm in the UV-vis absorption study, and the calculated excitonic band gap was 3.37 eV. The biosynthesized ZnO was used as a photocatalyst to remove the biohazardous safranin-O (SO) dye using solar irradiation. Freundlich isotherm model was used to study the adsorption behavior of SO onto ZnO. At optimum conditions, nearly 96.89% of the dye was degraded in just 80 minutes. Furthermore, the impact of catalyst dose, initial dye concentration, solution pH, and temperature on photodegradation was also investigated.

Keywords: Biosynthesis, *Borassus flabellifer*, Zinc oxide, Photocatalysis, Optimization, Safranin-O.

Introduction

ZnO nanoparticles are n-type II-IV semiconductors with exceptional properties like large excitonic binding energy, sizeable direct band gap, and excellent chemical and structural stability. The unique properties (Parimala & Ganeshkumar, 2024) of ZnO nanostructures make them useful in several applications, including the production of optoelectronic devices (Mirzaei & Darroudi, 2017), photovoltaics (Manasa *et al.*, 2021), biosensors (Liu *et al.*,

2020), solar cells (Barman *et al.*, 2020), and energy storage devices (Ba-Abbad *et al.*, 2017). Several methods are used to fabricate ZnO nanostructures, e.g., sol-gel (Ba-Abbad *et al.*, 2013), chemical precipitation (Suwanboon *et al.*, 2013), hydrothermal (Yu *et al.*, 2013), sonochemical [(Mishra *et al.*, 2010), combustion (Kooti & Sedeh, 2013), electrodeposition (Yang *et al.*, 2015), pyrolysis (Cho *et al.*, 2019) and biosynthesis (Sorbiun *et al.*, 2018). The biosynthesis process has several advantages over physical/chemical methods. This method is simple, eco-friendly, low-cost, and has a large-scale production possibility. It does not need additional chemicals and is stable and biocompatible. Natural components such as plant parts, fungi, bacteria, and enzymes stabilize and reduce agents during biosynthesis in place of chemicals (Selim *et al.*, 2020). Therefore, the green synthesis of ZnO-NPs has received extensive attention from researchers, and many groups are working on green synthesis.

Nowadays, wastewater is an increasingly significant challenge. Due to industrialization, several organic dyes (Arthanareeswar *et al.*, 2029) have been used in diverse industries, such as fabric, paper, cosmetics, drugs, food coloring, paints, ceramics, leather, and hair coloring products (Zhu *et al.*, 2011). Safranin-O (SO) is one of the most prevalent dyes found in industrial effluent. It is a reddish-brown water-soluble powder, initially a phenazine dye utilized in fabric, paper, and leather manufacturing (Alamgir & Alamgir, 2017). The SO dye was also used in biology labs. When SO is

¹Department of Physics, Bankura Zilla Saradamani Mahila Mahavidyalaya, Bankura University, Bankura, West Bengal, India.

²Department of Physics, Ramananda College, Bankura, West Bengal, India.

***Corresponding Author:** Goutam Mandal, Department of Physics, Bankura Zilla Saradamani Mahila Mahavidyalaya, Bankura University, Bankura, West Bengal, India., E-Mail: phy.gmandal@gmail.com

How to cite this article: Mandal, G., Bhattacharjee, B. (2024). Biosynthesis of ZnO nanoparticles using the young fruit of *Borassus flabellifer*: Characterization and photocatalytic removal of biohazardous safranin-O dye using solar irradiation. The Scientific Temper, **15**(2):2092-2098.

Doi: 10.58414/SCIENTIFICTEMPER.2024.15.2.19

Source of support: Nil

Conflict of interest: None.

present, it causes mouth, tongue, throat, and lip discomfort and stomach pain, leading to nausea, vomiting, and diarrhea (Bekkouche *et al.*, 2017). Thus, removing SO dye from the wastewater is essential for environmental health.

Adsorptions and chemical coagulations are some common approaches for the remediation of wastewater. But these techniques convert dyes from liquid to solid state. Thus, extra processing is required to remove secondary pollutants (Saravanan *et al.*, 2021). Photocatalysis emerged as a potential method for removing organic contaminants from wastewater since it is easy, economical, efficient, and environmentally benign. In photocatalysis, the photocatalyst takes in energy and forms electron-hole pairs (EHP), resulting in redox reactions at the catalyst surface that produce superoxide ($\cdot\text{O}_2^-$) and hydroxyl radical ($\cdot\text{OH}$). These $\cdot\text{O}_2^-$ and $\cdot\text{OH}$ radicals are responsible for breaking down hazardous pollutants in wastewater (Pandis *et al.*, 2022). Nano photocatalysts such as ZnO have the potential to degrade SO dye into a harmless compound.

Borassus flabellifer (Palmyra palm) belongs to the Arecaceae family and is often found in India, Bangladesh, Thailand, and Sri Lanka, among other places. *B. flabellifer* is commonly used as a stimulant, antileprotic, diuretic, and antiphlogistic. Studies show no biosynthesis of ZnO NPs has been fabricated utilizing *B. flabellifer* young fruit extract (BFFE).

Considering all in mind, the present work focuses on synthesizing ZnO NPs using the young fruit of *B. flabellifer*. Microstructures were studied using X-ray diffraction (XRD), field-emission scanning electron microscope (FESEM), and UV-vis spectrophotometer and the photocatalytic performance against SO pollutants using solar light.

Materials and Methods

Materials

The zinc nitrate hexahydrate and sodium hydroxide were obtained from Sigma-Aldrich and used for synthesis with no treatment. The safranin-O dye was purchased from SRL, India. A stock solution of SO dye with a concentration of 1 g/L was ready and diluted to the appropriate concentration by mixing deionized water.

Preparation of Young Fruit Extract of BFFE

The young fruits of *B. flabellifer* were collected from the local area of the district of Bankura (23.1645° N, 87.0624°E), West Bengal, India. Initially, a young fruit of *Borassus flabellifer* was washed two or three times in pure water to clean the contaminants, like sand, dust, etc., from the outer surface. Then, fruits were cut, and the thick white jelly-like part (ice apple) was collected by removing the coating surface of the ice apple. About 15 g of the jelly was mixed in 100 mL of distilled water and stirred at 60°C for 15 minutes. Finally, the aqueous part was separated with filter paper and stored in a conical flask in a refrigerator till future work.

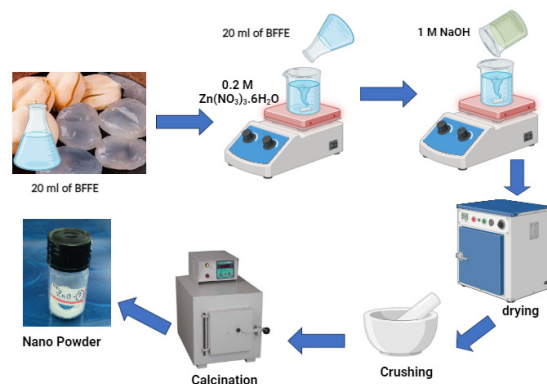


Figure 1: Schematic biosynthesis process of ZnO nanocatalyst

Biosynthesis of ZnO Nanoparticles

At first, a 0.2 M aqueous solution of zinc nitrate hexahydrate was prepared by dissolving 5.95 g zinc nitrate in 50 mL deionized water. Beforehand, 20 mL of BFFE was added to the zinc acetate dihydrate solution under a magnetic stirrer. After 30 Minutes, 30 mL of 1M NaOH was mixed into the solution and agitated for 3 hours. At the end of the process, a white precipitate was formed. The precipitate was filtered through filter paper, washed with ethanol, and deionized water several times. The precipitate was dried in a hot air oven at 50°C and crushed with a ceramic pestle and mortar to get fine powder. Then, the powder finally calcinated at 250°C for 4 hours. The schematic synthesis process is given in Figure 1.

Instruments

A dual-beam UV-vis spectrophotometer (Model: Systronics AU-2703) was used to study the optical absorption. X-ray diffraction data was collected in a Rigaku XRD machine using Cu-K α ($\lambda = 1.54 \text{ \AA}$) radiation and an angular selection of $20^\circ < 2\theta < 80^\circ$. The surface morphology of the catalysts was explored using a FESEM (Make: ZEISS) at 5 kV accelerating voltages.

Photodegradation Study

The dye removal performance was investigated by photodegrading 100 mL SO aqueous solution (40 mg/L) at a catalyst dose of 0.3 g/L with solar irradiation. The organic structure and other details of SO dye are shown in Table 1. The progress of photodegradation was studied by recording UV-vis absorption data at regular intervals and by monitoring the primary peak of SO dye at $\lambda_{max} = 520 \text{ nm}$. The effects of operating parameters such as photocatalyst dose, SO concentration, pH of the solution, and temperature were chosen for the study. To adjust the pH of the solution, 0.1M HCl or NaOH was added as per the requirements. The photodegradation efficiency (η) of the photocatalyst was measured by the following formula (Meng *et al.*, 2009):

$$\eta \% = \frac{C_0 - C_t}{C_0} \times 100\% \quad (1)$$

Table 1: Properties of SO dye

Material	Chemical structure	λ_{max} (nm)	MW(g/ mol)	Formula	Solubility (g/L)
Safranin-O		520	350.85	$C_{20}H_{19}N_4Cl$	1

Here, C_0 and C_t are the initial and dye concentrations at any time t of irradiation.

Results and Discussion

Absorption Spectra

The wavelength (λ) ranging from 200 to 800 nm of the UV-vis spectrophotometer was used to determine the absorption peak and the optical band gap E_g . Here, Figure 2(A) shows the optical absorption spectrum of the grown zinc oxide nanocrystal dispersed in distilled water. A sharp absorption peak is seen at $\lambda \approx 375$ nm.

The band gap (E_g) of the nanoparticles was estimated using the Tauc equation (Tauc, 1966):

$$(\alpha h\nu)^2 = B(h\nu - E_g) \quad (2)$$

Here, h : Planck's constant, ν : frequency, B : band tailing parameter. Hence, using the plot of $(\alpha h\nu)^2$ vs. energy $h\nu$, the band gap energy E_g was determined from the linear part of the graph. Figure 2(B) illustrates the method for determination of band gap E_g of the fabricated nanocrystal. The direct band gap was calculated and found to be 3.79 eV.

FESEM Analysis

From the FESEM image (Figure 3), the surface morphology, the size of the crystallite, and the shape and growth mechanism of the ZnO nanocrystal have been studied. The FESEM image shows that fabricated nanoparticles are spherical and randomly oriented. The size distribution is random, ranging from 26 to 43 nm. The mean nanoparticle size was calculated using ImageJ software and found to be 38.76 nm.

Crystallinity Analysis from X-ray Diffraction

XRD pattern of the biosynthesized zinc oxide nanocrystal is shown in Figure 4(A). According to XRD data, the unit cell of synthesized ZnO nanocrystals is wurtzite hexagonal,

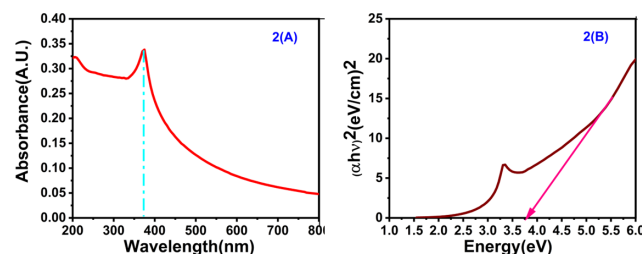


Figure 2: (A) Absorption spectra of biosynthesized ZnO, (B) Tauc's plot

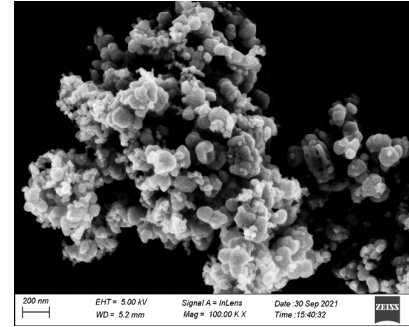


Figure 3: FESEM image of green synthesized ZnO nanocrystal

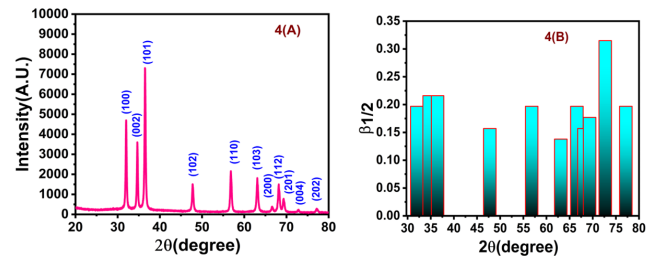


Figure 4: (A) The XRD pattern of the ZnO nanocrystal (B) Variation of FWHM ($\beta_{1/2}$) of the different peaks with peak position (2θ)

with peak positions (2θ) at (100), (002), (101), (102), (110), (103), (200), (112), (201), (004) and (202). Out of all peaks, the (004) and (202) peaks have very poor intensities compared to other peaks. The planes are randomly oriented, as seen from the diffraction pattern (Liang *et al.*, 2019). The peaks in the XRD spectra strongly match (JCPDS file no. 96-210-7060) with the hexagonal (wurtzite) phase with space group $P6_3mc$, and the lattice constants are $a = b = 3.242 \text{ \AA}$ and $c = 5.188 \text{ \AA}$. Figure 4(B) illustrates the variation of FWHM or half-width ($\beta_{1/2}$) vs. diffraction peaks (2θ). Gaussian fitting was used to obtain the FWHM of each diffraction peak. At $2\theta = 36.454 \text{ \AA}$, the nanocrystal exhibits the maximum peak intensity associated with (101) Miller plane, which was taken to determine the crystallographic parameters.

Debye-Scherrer relations (Abu-Dief & Mohamed, 2027) are used to determine the average grain size (D_V), the dislocation density (δ_D), and the microstrain (ϵ_m) of the nanocrystal using the following equations:

$$D_V = \frac{K\lambda}{\beta_{1/2} \cos\theta} \quad (3)$$

$$\delta_D = \frac{1}{D_V^2} \quad (4)$$

$$\epsilon_m = \frac{\beta_{1/2} \cos\theta}{4} \quad (5)$$

For copper radiation, the value of $K = 0.94$.

Williamson-Hall (W-H) equation (Kahouli *et al.*, 2015) was also used to calculate the microstrain (ϵ_m) and crystallite grain size (D_V) of the nanocrystal and is given by:

$$\beta_{1/2} \cos\theta = \frac{K\lambda}{D_V} + 4\epsilon_m \sin\theta \quad (6)$$

Table 2: Different crystal parameters

Scherrer's method [considering (101) plane]			Williamson–Hall method		
Grain size (D_p)	Microstrain (ϵ_m)	Dislocation density (δ_p)	Grain size (D_p)	Microstrain (ϵ_m)	Dislocation density (δ_p)
40.43 nm	0.000825	0.000618	39.83 nm	0.000895	0.000715

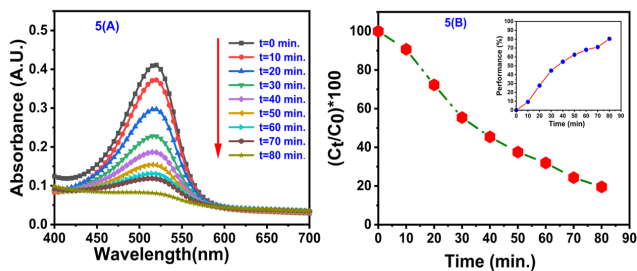


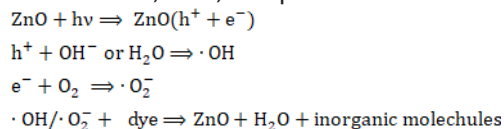
Figure 5: UV-vis absorption spectra of (A) SO dye (concentration 40 mg/L) on irradiation with white light about 80 min., (B) $\frac{C_t}{C_0}$ vs. time plot (photodegradation performance vs. time plot inset)

The evaluated values of different crystal parameters are shown in Table 2.

Photodegradation of SO Dye

Several studies have been carried out to determine how molecular structure and functional groups influence photodegradation (Shams *et al.*, 2019). The photocatalyst dose of 0.3 g/L and the SO dye concentration of 40 mg/L (100 mL solution) were taken to study the photodegradation efficiency. The photodegradation of SO dye is shown in Figure 5(A). The percentage degradation after 80 minutes of irradiation was 80.44%. The photodegradation efficiency with time is depicted in Figure 5(B).

When photon energy E is larger than the band gap energy (E_g) of the photocatalyst, then electrons (e^-) and holes (h^+) are produced. These photogenerated holes (h^+) either directly oxidize the organic dye or interact with water molecules (H_2O) or hydroxyl ions (OH^-) produces hydroxyl radicals ($\cdot OH$). Also, photogenerated electrons (e^-) are reacted with the oxygen molecules present on the photocatalyst surface, reduce them to produce superoxide radicals ($\cdot O_2^-$). The generated $\cdot OH$ radicals and superoxide (O_2^-) degrades the organic dye into inorganic molecules (Nenavathu *et al.*, 2018). The photoreaction is shown below:



The schematic diagram of the photocatalysis process is given in Figure 6.

Photodegradation kinetics

Using the pseudo-first-order Langmuir-Hinshelwood model (Moradi *et al.*, 2018) kinetic model, the apparent reaction constant (k_{ap}) for the photodegradation was calculated using the following equation:

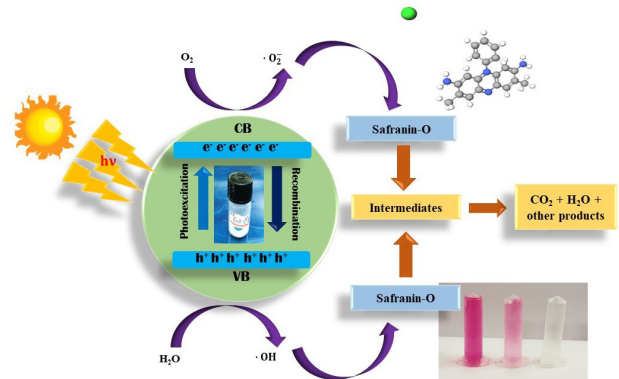


Figure 6: Schematic diagram of photodegradation of SO dye

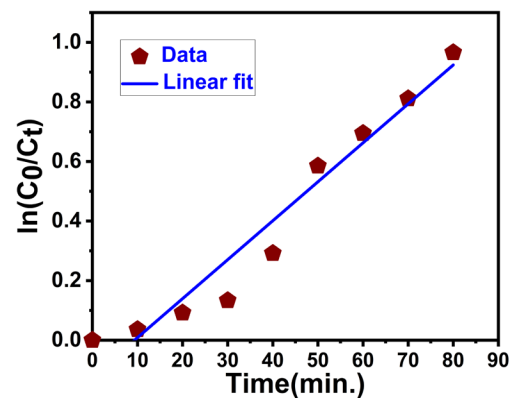


Figure 7: Plot to determine the rate constant of SO dye (concentration: 50 mg/L) on irradiation for 80 minutes

$$\ln\left(\frac{C_0}{C_t}\right) = k_{ap} t \quad (9)$$

From the plot of $\ln\left(\frac{C_0}{C_t}\right)$ vs. time t , we can determine k_{ap} (min^{-1}) using the slope of the straight portion of the curve (Figure 7). In our study, we got the rate constant was 0.00976 min^{-1} .

Catalyst dose on photodegradation

The generation of hydroxyl ($\cdot OH$) radicals increases with optimal ZnO dose, resulting in efficient photodegradation. Here, the dose of the photocatalyst varies from 0.1 to 1.0 g/L, keeping the dye strength at 40 mg/L and the pH at 7. Decolorization was studied after 80 minutes of solar irradiation. The photodegradation of SO dye with photocatalyst doses and the corresponding bar diagram are shown in Figures 8(A) and 8(B), respectively. On raising the dose of ZnO photocatalyst, the degradation rate also increases. The maximum degradation we found was 91.32%

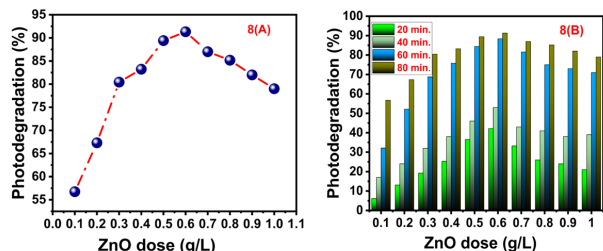


Figure 8: (A) Effect of ZnO doses on degradation of SO (SO dye concentration 50 mg/L and pH: 7), (B) The corresponding bar diagrams under irradiation time for 80 minutes

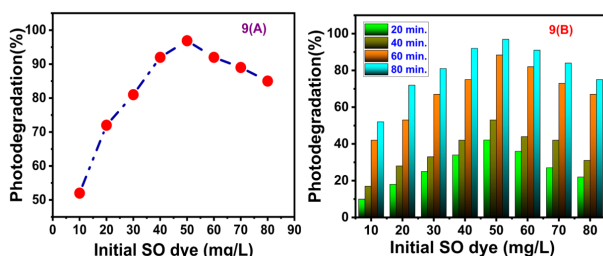


Figure 9: The variation of photodegradation percentage with the initial dye concentration with photocatalysts dose 0.6 g/L for SO and pH: 7, under irradiation time of 80 minutes

when the photocatalyst dose was 0.6 g/L. After that, the increase in photocatalyst concentration resulted in low degradation.

When the photocatalyst dose increases, the quantity of active sites on the photocatalyst's surface increases, increasing the number of hydroxyl ($\cdot\text{OH}$) radicals. But, after a certain amount, increasing the photocatalyst dose shows adverse effects, i.e., percentage degradation decreases. On further increasing photocatalyst doses, the catalyst particles are gathered in the solution. This accumulation of the catalyst prevents the light from reaching the inner surface of the photocatalyst (Weon & Choi, 2019).

Initial dye concentration on photodegradation

In this study, the initial SO dye concentration was varied from 10 to 80 mg/L in the step of 10 mg/L, keeping the photocatalyst at its optimum concentration, i.e., 0.6 g/L. The efficiency initially increases with the initial dye concentration, reaches the optimum value, and then decreases with further increase in dye concentrations (Figure 9(A) and 9(B)). The highest percentage of degradation was found at 96.89% at a dye concentration of 50 mg/L.

This may be due to the hindering of light penetration in the liquid, which prevents photons from approaching the catalyst's surface. As a result, the number of photogenerated EHP decreased, and degradation was also lower. Furthermore, the increased dye molecules masked the active sites on the catalyst's surface. Hence, only some reactive sites will be accessible to generate EHP that generate $\cdot\text{OH}$ and $\cdot\text{O}_2^-$, which are in control for the degradation of SO dye.

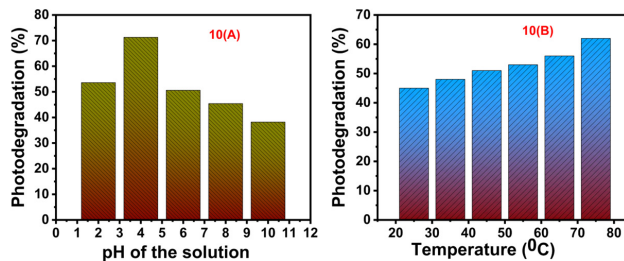


Figure 10: The variation of photodegradation percentage with (A) pH of the solution, (B) temperature of the solution under irradiation time of 40 minutes

pH of the solution on photodegradation

The photocatalytic degradation of dye is significantly affected by the pH of the dye solution (Krishnakumar *et al.*, 2010). The acid-base characteristics of the surface of photocatalysts can dramatically affect their photocatalytic activity (He, 2017). From pH 2 to 10, the impact of pH on photodegradation was investigated using a dye concentration of 50 mg/L, 0.6 g/L photocatalyst dose, and a 40 minutes irradiation time. The percentage degradation was 53.6% at pH 2, rising to 71.7% at pH 4 and then falling to 38.2% at pH 10 (Figure 10(A)). A reaction between holes and hydroxide ions produces $\cdot\text{OH}$ radicals. At low pH, holes are the main oxidizing species, but at neutral or higher pH, $\cdot\text{OH}$ radicals are the predominant species. Furthermore, a higher degradation rate indicates that the species causing the deterioration are holes.

Effect of temperature

The effect of temperature (range 25–75°C) on the degradation of the SO dye with ZnO NPs is presented in Figure 10(B). The study was conducted for 40 minutes of irradiation with optimum photocatalyst and SO dye concentration. It has been observed that higher temperatures accelerate the breakdown of dye, resulting in a maximum degradation of 61 at 75°C. The temperature usually doesn't have much of an effect on photodegradation. However, if the temperature is raised, it can speed up the electron-hole recombination process, which can lead to the completion of the reaction and the photodegradation of the dye (Khan *et al.*, 2020). Thus, a higher temperature promotes a faster reaction rate for dye removal.

Conclusion

The current research looks at the synthesis of ZnO nanocrystals through the green route and studies its ability as a photocatalyst. Here, we have effectively synthesized ZnO nanocrystals using the young fruit of *B. flabellifer*. Characterize the synthesized nanoparticles employing UV-Vis spectroscopy, FESEM, and XRD techniques. The spherical nanoparticles with a mean particle size of 39.83 nm

and optical band gap of 3.39 eV were found in the microstructure study. The adsorption and photodegradation performance of synthesized ZnO NPs was studied on SO wastewater pollutants for the 1st time. The photodegradation of SO dye under solar light illumination after 80 minutes was 96.89% at optimum conditions. Thus, our green synthesized ZnO using *B. flabellifer* has the potential for the rapid degradation of SO dye in the presence of sunlight, as well as for wastewater treatment and environmental improvements.

Acknowledgment

The authors thank the Department of Physics, Bankura University, and Bankura Zilla Saradamani Mahila Mahavidyapith.

References

- Abu-Dief, A. M., & Mohamed, W. S. (2017). α -Bi₂O₃ nanorods: synthesis, characterization and UV-photocatalytic activity. *Materials Research Express*, 4(3), 035039.
- Abu-Dief, A. M., & Mohamed, W. S. (2017). α -Bi₂O₃ nanorods: synthesis, characterization and UV-photocatalytic activity. *Materials Research Express*, 4(3): 035039.
- Alamgir, A. N. M. (2017). *Therapeutic use of medicinal plants and their extracts: volume 1*. Springer International Publishing AG..
- Arthanareeswari, M., Devikala, S., & Sridharan, M. (2019). Green synthesis of zinc oxide nanoparticles using *Typha latifolia*. L leaf extract for photocatalytic applications. *Materials Today: Proceedings*, 14, 332-337.
- Ba-Abbad, M. M., Kadhum, A. A. H., Mohamad, A. B., Takriff, M. S., & Sopian, K. (2013). The effect of process parameters on the size of ZnO nanoparticles synthesized via the sol-gel technique. *Journal of Alloys and Compounds*, 550, 63-70.
- Ba-Abbad, M. M., Takriff, M. S., Benamor, A., Mahmoudi, E., & Mohammad, A. W. (2017). Arabic gum as green agent for ZnO nanoparticles synthesis: properties, mechanism and antibacterial activity. *Journal of Materials Science: Materials in Electronics*, 28, 12100-12107.
- Barman, S., Sikdar, S., Biswas, A., Mandal, B. K., & Das, R. (2020). Structural microanalysis of green synthesized Al_xZn (1-x) O nanoparticles. *Nano Express*, 1(2), 020003.
- Bekkouche, S., Merouani, S., Hamdaoui, O., & Bouhelassa, M. (2017). Efficient photocatalytic degradation of Safranin O by integrating solar-UV/TiO₂/persulfate treatment: Implication of sulfate radical in the oxidation process and effect of various water matrix components. *Journal of Photochemistry and Photobiology A: Chemistry*, 345, 80-91.
- Cho, J., Hwang, S., Ko, D. H., & Chung, S. (2019). Transparent ZnO thin-film deposition by spray pyrolysis for high-performance metal-oxide field-effect transistors. *Materials*, 12(20), 3423.
- He, H. Y. (2017). Efficient interface-induced effect of novel reduced graphene oxide-CoS heteronanostructures in enhancing photocatalytic activities. *Applied Surface Science*, 421, 260-267.
- Kahouli, M., Barhoumi, A., Bouzid, A., Al-Hajry, A., & Guermazi, S. (2015). Structural and optical properties of ZnO nanoparticles prepared by direct precipitation method. *Superlattices and Microstructures*, 85, 7-23.
- Khan, F., Khan, M. S., Kamal, S., Arshad, M., Ahmad, S. I., & Nami, S. A. (2020). Recent advances in graphene oxide and reduced graphene oxide based nanocomposites for the photodegradation of dyes. *Journal of Materials Chemistry C*, 8(45), 15940-15955.
- Kooti, M., & Sedeh, A. N. (2013). Synthesis and characterization of NiFe₂O₄ magnetic nanoparticles by combustion method. *Journal of Materials Science & Technology*, 29(1), 34-38.
- Krishnakumar, B., Selvam, K., Velmurugan, R., & Swaminathan, M. (2010). Influence of operational parameters on photodegradation of Acid Black 1 with ZnO. *Desalination and Water Treatment*, 24(1-3), 132-139.
- Liang, Q., Qiao, F., Cui, X., & Hou, X. (2019). Controlling the morphology of ZnO structures via low temperature hydrothermal method and their optoelectronic application. *Materials Science in Semiconductor Processing*, 89, 154-160.
- Liu, Z. Y., Shen, C. L., Lou, Q., Zhao, W. B., Wei, J. Y., Liu, K. K., ... & Shan, C. X. (2020). Efficient chemiluminescent ZnO nanoparticles for cellular imaging. *Journal of Luminescence*, 221, 117111.
- Manasa, D. J., Chandrashekar, K. R., Kumar, D. M., Niranjana, M., & Navada, K. M. (2021). Mussaenda frondosa L. mediated facile green synthesis of copper oxide nanoparticles-characterization, photocatalytic and their biological investigations. *Arabian journal of chemistry*, 14(6), 103184.
- Meng, F., Song, X., & Sun, Z. (2009). Photocatalytic activity of TiO₂ thin films deposited by RF magnetron sputtering. *Vacuum*, 83(9), 1147-1151.
- Mirzaei, H., & Darroudi, M. (2017). Zinc oxide nanoparticles: Biological synthesis and biomedical applications. *Ceramics International*, 43(1), 907-914.
- Mishra, P., Yadav, R. S., & Pandey, A. C. (2010). Growth mechanism and photoluminescence property of flower-like ZnO nanostructures synthesized by starch-assisted sonochemical method. *Ultrasonics sonochemistry*, 17(3), 560-565.
- Moradi, B., Nabiyouni, G., & Ghanbari, D. (2018). Rapid photodegradation of toxic dye pollutants: green synthesis of mono-disperse Fe₃O₄-CeO₂ nanocomposites in the presence of lemon extract. *Journal of Materials Science: Materials in Electronics*, 29, 11065-11080.
- Nenavathu, B. P., Kandula, S., & Verma, S. (2018). Visible-light-driven photocatalytic degradation of safranin-T dye using functionalized graphene oxide nanosheet (FGS)/ZnO nanocomposites. *RSC advances*, 8(35), 19659-19667.
- Pandis, P. K., Kalogirou, C., Kanellou, E., Vaitis, C., Savvidou, M. G., Sourkouni, G., ... & Argiris, C. (2022). Key points of advanced oxidation processes (AOPs) for wastewater, organic pollutants and pharmaceutical waste treatment: A mini review. *ChemEngineering*, 6(1), 8.
- Parimala, V., & Ganeshkumar, D. (2024). Solar energy-driven water distillation with nanoparticle integration for enhanced efficiency, sustainability, and potable water production in arid regions. *The Scientific Temper*, 15(01), 1644-1651.
- Saravanan, A., Kumar, P. S., Jeevanantham, S., Karishma, S., Tajsabreen, B., Yaashikaa, P. R., & Reshma, B. (2021). Effective water/wastewater treatment methodologies for toxic pollutants removal: Processes and applications towards sustainable development. *Chemosphere*, 280, 130595.
- Selim, Y. A., Azb, M. A., Ragab, I., & HM Abd El-Azim, M. (2020). Green synthesis of zinc oxide nanoparticles using aqueous extract of *Deverra tortuosa* and their cytotoxic activities. *Scientific reports*, 10(1), 3445.
- Shams, M., Guiney, L. M., Huang, L., Ramesh, M., Yang, X., Hersam, M. C., & Chowdhury, I. (2019). Influence of functional groups

- on the degradation of graphene oxide nanomaterials. *Environmental Science: Nano*, 6(7), 2203-2214.
- Sorbiun, M., Shayegan Mehr, E., Ramazani, A., & Mashhadi Malekzadeh, A. (2018). Biosynthesis of metallic nanoparticles using plant extracts and evaluation of their antibacterial properties. *Nanochemistry Research*, 3(1), 1-16.
- Suwanboon, S., Amornpitoksuk, P., Sukolrat, A., & Muensit, N. (2013). Optical and photocatalytic properties of La-doped ZnO nanoparticles prepared via precipitation and mechanical milling method. *Ceramics International*, 39(3), 2811-2819.
- Tauc, J., Grigorovici, R., & Vancu, A. (1966). Optical properties and electronic structure of amorphous germanium. *physica status solidi (b)*, 15(2), 627-637.
- Weon, S., He, F., & Choi, W. (2019). Status and challenges in photocatalytic nanotechnology for cleaning air polluted with volatile organic compounds: visible light utilization and catalyst deactivation. *Environmental Science: Nano*, 6(11), 3185-3214.
- Yang, J., Wang, Y., Kong, J., Jia, H., & Wang, Z. (2015). Synthesis of ZnO nanosheets via electrodeposition method and their optical properties, growth mechanism. *Optical Materials*, 46, 179-185.
- Yu, A., Qian, J., Pan, H., Cui, Y., Xu, M., Tu, L., ... & Zhou, X. (2011). Micro-lotus constructed by Fe-doped ZnO hierarchically porous nanosheets: preparation, characterization and gas sensing property. *Sensors and Actuators B: Chemical*, 158(1), 9-16.
- Zhu, H. Y., Fu, Y. Q., Jiang, R., Jiang, J. H., Xiao, L., Zeng, G. M., ... & Wang, Y. (2011). Adsorption removal of congo red onto magnetic cellulose/Fe₃O₄/activated carbon composite: Equilibrium, kinetic and thermodynamic studies. *Chemical Engineering Journal*, 173(2), 494-502.